Investigation of dose uniformity on the inner races of bearings treated by plasma immersion ion implantation

Z. M. Zeng,[a] T. K. Kwok, X. B. Tian,[a] B. Y. Tang,[a] and P. K. Chu[b]
Department of Physics and Material Science, City University of Hong Kong, 83 Tat Chee Avenue, Kowloon, Hong Kong

(Received 7 December 1998; accepted for publication 30 March 1999)

Plasma immersion ion implantation (PIII) is an effective technique for the surface modification of industrial components possessing an irregular shape. We have recently used PIII to treat a real industrial ball bearing to enhance the surface properties of the race surface on which the balls roll. The implantation dose uniformity along the groove is assessed using theoretical simulation and experiments. The two sets of results agree very well, showing larger doses near the center. However, the highest dose is not observed at the bottom or center of the groove, but rather offset toward the side close to the sample platen when the bearing is placed horizontally. The minimum dose is observed near the edge or corner of the groove and our model indicates that it is due to the more glancing ion incidence as a result of the evolution of the ion sheath near the corner. The dose nonuniformity along the groove surface is about 40% based on our experimental data. © *1999 American Institute of Physics.* [S0021-8979(99)06013-2]

I. INTRODUCTION

Plasma immersion ion implantation (PIII) is a burgeoning non-line-of-sight technique for the surface modification of industrial components.[1–3] One of the advantages over ion beam implantation techniques is its ability to rapidly treat objects possessing an irregular shape.[4] Moreover, as there are almost no dimensional changes after implantation, the technique is a very effective way to enhance the surface properties of mechanical parts having strict dimensional tolerances such as precision bearings.[5] The viability of the PIII technique in an industrial environment hinges on the uniformity of the implantation dose along the working surface. For a ball bearing, the balls can be implanted quite uniformly to achieve a better surface sturdiness and lower friction, but uniform implantation along the inner and outer races is much more complicated. In the work described in this article, we conduct a systematic investigation on the implantation dose uniformity on the arc race of a real ball bearing experimentally and using theoretical simulation. The work is aimed at a better understanding of the treatment process for industrial bearings as well as the plasma sheath evolution in the vicinity of a groove.

II. EXPERIMENT

An industrial bearing with an inner race (Chinese model 310) shown in Fig. 1 was treated in a multipurpose plasma immersion ion implanter.[6] The interior diameter of the 9Cr18 stainless steel bearing was 50 mm. Before implantation, five 2 mm×3 mm stainless steel sheets were affixed along the groove with silver conductive glue for Auger measurements. They are labeled 1 through 5 in Fig. 2. The bearing was placed horizontally on a 2 mm thick copper platen having the same diameter. The platen was connected to the sample stage in the vacuum chamber by an aluminum rod 6 mm in diameter and 500 mm long to establish electrical contact. To minimize the influence of the sample stage, a glass shroud was used to cover the rod. The vacuum chamber was pumped down to a base pressure of 8×10^{-4} Pa before a nitrogen plasma was ignited using a filament source. The experimental conditions are summarized in Table I. The implanted stainless steel sheets were analyzed using Auger electron spectroscopy (AES) to obtain the nitrogen depth profile and calculate the implantation dose at the five locations along the groove surface.

III. THEORETICAL SIMULATION

The implantation uniformity is investigated by simulating the temporal sheath expansion using a two-dimensional fluid model. The target is immersed in a plasma with density n_0 and potential $\phi=0$. The plasma density is assumed to be spatially uniform before each voltage pulse. At time $t=0$, the target potential is switched from $\phi=0$ to a negative potential $\phi=\phi_t$. An ion-matrix sheath is subsequently induced. When $t>\omega_{pe}^{-1}$ (inverse electron plasma frequency), ions are accelerated by the electric field and implanted into the target until the applied voltage pulse is over. The evolution of ion densities n_i, ion velocity v_i, and electric potential ϕ can be modeled using cold, collissionless fluid ions, Boltzmann electrons and Poisson's equation.[7–12] In cylindrical coordinates, the two-dimensional equations of ion continuity and motion, Poisson's equation and Boltzmann relation are

$$\frac{\partial n}{\partial \tau}+\frac{1}{R}\frac{\partial}{\partial R}(Rnu_R)+\frac{\partial}{\partial Z}(nu_Z)=0, \tag{1}$$

$$\frac{\partial u_R}{\partial \tau}+u_R\frac{\partial}{\partial R}+u_Z\frac{\partial u_R}{\partial Z}=\frac{1}{2}\frac{\partial \psi}{\partial R}, \tag{2a}$$

[a]Also with Advanced Welding Production & Technology National Key Lab, Harbin Institute of Technology, Harbin, People's Republic of China
[b]Corresponding author; electronic mail: paul.chu@cityu.edu.hk

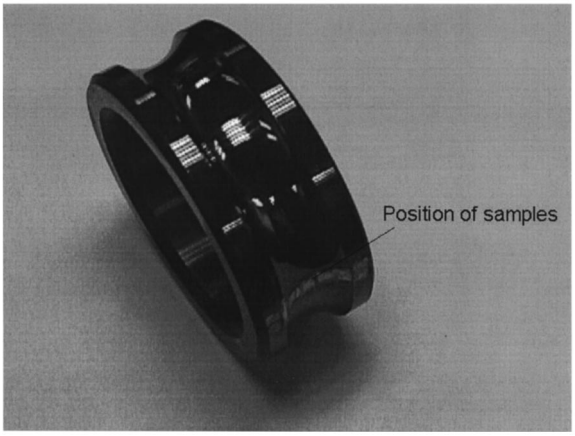

FIG. 1. Photograph of the treated bearing. The five ''white'' square spots on the bottom show the locations where the five 2 mm×3 mm stainless steel sheets were originally affixed. The five sheets were subsequently measured by Auger to obtain the projected ranges and retained doses (see Fig. 7).

$$\frac{\partial u_Z}{\partial \tau}+u_R\frac{\partial u_Z}{\partial R}+u_Z\frac{\partial u_Z}{\partial Z}=\frac{1}{2}\frac{\partial \psi}{\partial Z}, \tag{2b}$$

$$\frac{\partial^2 \psi}{\partial R^2}+\frac{1}{R}\frac{\partial \psi}{\partial R}+\frac{\partial^2 \psi}{\partial Z^2}=2\left[n-\exp\left(\frac{e\phi_t}{KT_e}\psi\right)\right]. \tag{3}$$

The dimensionless variables are

$$R=x/s_0 \quad Z=z/s_0, \quad \psi=\phi/\phi_t, \quad n=n_i/n_0,$$

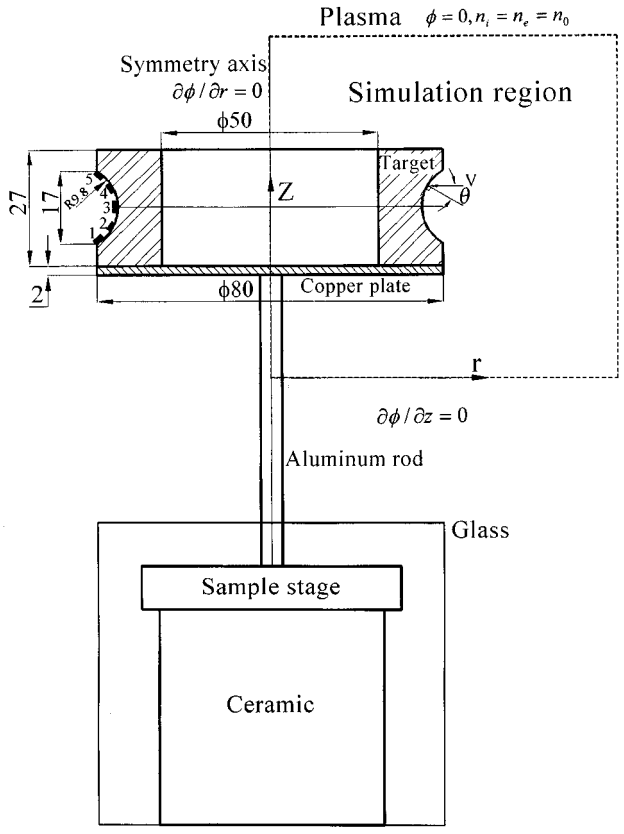

FIG. 2. Schematic of the experimental setup and simulation region (dimensions in mm).

TABLE I. Experimental parameters of the PIII treatment process.

Implantation voltage	−20 kV
Pulse width	10 μs
Pulse repetition rate	300 Hz
Gas pressure	2.2×10^{-2} Pa
Filament discharge current	1 A
Filament discharge voltage	90 V
Measured plasma density	3.5×10^{9} cm^{-3}
Measured electron temperature	1.4 eV
Implantation time	3 h

$$u_R=v_{ir}/v_{\max}, \quad u_Z=v_{iz}/v_{\max}, \quad \tau=t\bar{\omega}_{pi}, \tag{4}$$

where $s_0=\sqrt{-2\varepsilon_0\phi_t/en_0}$ is the planar ion ion-matrix sheath width, $v_{\max}=\sqrt{-2e\phi_t/m}$ is the velocity that an ion would gain if it fell through a potential drop ϕ_t, and $\varpi_{pi}=\sqrt{n_0e^2/\varepsilon_0 m}$ is the ion plasma frequency.

The simulation regions are depicted in Fig. 2. The initial conditions are $n=1$ and $u_R=u_z=0$ everywhere. The boundary conditions are $\psi=1$ on the target, $\psi=0$ in the plasma, $\partial\psi/\partial r=0$ at the center symmetry axis of the race, and $\partial\psi/\partial z=0$ on the lower boundary of the simulation region because it is far from the race and can be treated as a one-dimensional case.

The equations are solved by the finite difference method. The simulation parameters are chosen based on the real experimental parameters: $n_0=3.5\times10^9$ cm^{-3}, $\phi_t=-20$ kV, $kT_e=1.5$ eV, and nitrogen plasma. Hence, $s_0=25.1$ mm and $\omega_{pi}^{-1}=0.0678$ μs. We choose a grid spacing $h=\Delta R=\Delta Z=\frac{1}{32}s_0=0.784$ mm and a time step of $\Delta\tau=1/64$. The simulation region is chosen to be $8s_0$ in height and $5s_0$ in the radial direction, so that the sheath will remain inside it throughout the entire simulated time duration. The simulation is conducted to a final time $t=10$ μs ($\tau=147$). Because the arc boundary of the groove is a curved surface, not all of the boundary grid points are exactly on the target boundary. Hence, the values of the boundary grid points along the groove are calculated by the linear interpolating method with an error of 0 (h^2).

IV. RESULTS AND DISCUSSION

A. Simulation results

Figure 3 shows the potential distribution of the ion-matrix sheath formed at $\tau=0$. The $\psi=0.9$ potential contour nearly conforms to the target with a low curvature radius, but the $\psi=0$ contour has almost acquired a domed shape.

The working surface of the bearing is the arc groove on which the balls roll. Therefore, we only need to discuss the results in the groove. Figure 4 depicts the distribution and temporal evolution of the ion incident angle relative to the normal (for the groove, the normal direction is the radial direction). As expected, ions striking the area near the groove corner impact at the most glancing angle. Initially, the angle of incidence along the groove surface has small values (i.e., close to normal incidence) except close to the edge that has an angle of incidence of about 20° from the normal. In addition, the impact angle distributions at the upper and lower side are almost symmetrical in the beginning.

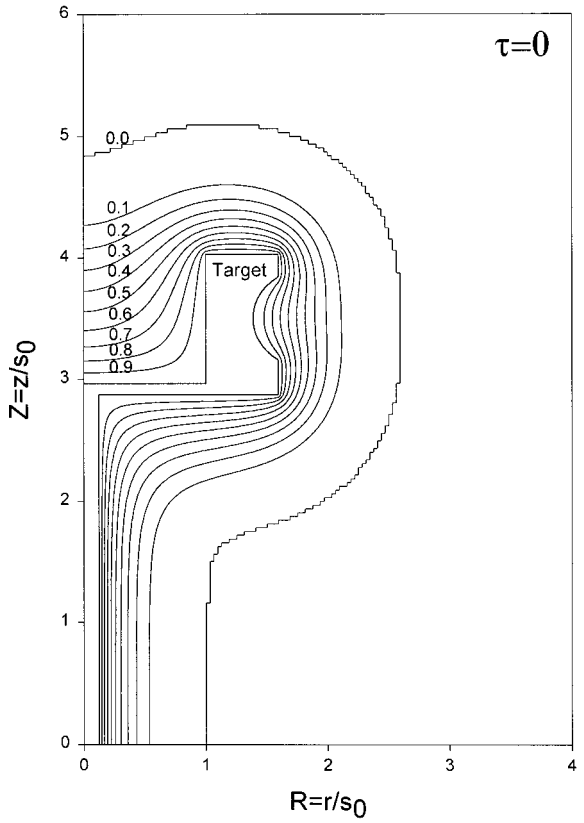

FIG. 3. Equipotential contours of the ion-matrix sheath formed at $t=0$.

However, it should be noted that in the early stage of sheath expansion, ions may not be accelerated by the full potential, and even though the angle of incidence is near normal, the implantation depth may be smaller than that during the latter stage of the sheath expansion. As the sheath expands, the incident ions become more and more oblique, except near the center of the groove. When $\tau=30$, the incident angle at the upper corner has reached nearly 70°. At a later time, the ion impinging near the corner becomes nearly parallel to the surface thereby resulting in more sputtering than implantation. The lower side is bombarded with ions impacting at a smaller angle due to the influence of the sample platen.

The incident ion dose $D(r,z)$ can be calculated by integrating the ion flux at the target surface:

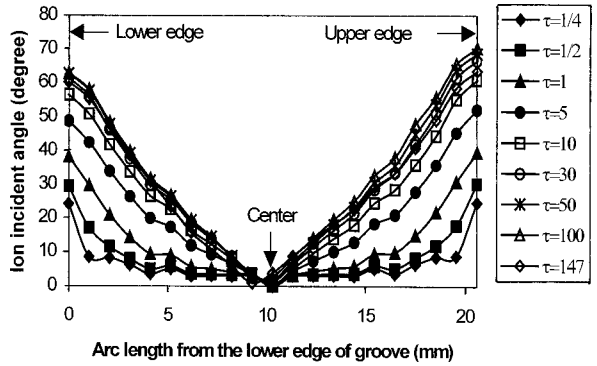

FIG. 4. Variation of the simulated incident angle distributions (from normal) along the groove surface with time.

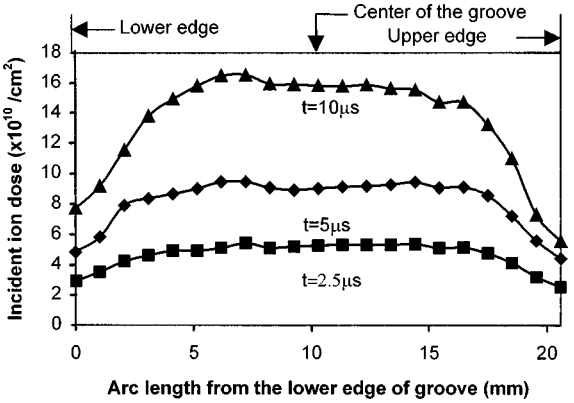

FIG. 5. Simulated distribution of incident ion dose along the bearing inner race surface at three different times.

$$D(r,z)=\int_0^{t_p} n_i(t,r,z)\,v_{i\perp}(t,r,z)\,dt$$

$$=\int_0^{t_p} n_i(t,r,z)\sqrt{(v_{ir}^2(t,r,z)+v_{iz}^2(t,r,z)}\cos\theta\,dt, \tag{5}$$

where t_p is pulse duration and $v_{i\perp}$ is the ion velocity normal to the target surface. The results are exhibited in Fig. 5. In calculating the dose, we have not taken into account any sputtering loss. As the sputtering loss depends on the impact angle, that is, more sputtering at glancing incidence, the net retained dose may deviate from the incident dose. However, as shown by our experimental data discussed in the next section, the difference is not big. A larger ion dose is observed near the groove center compared to the edges. Interestingly, the area with the largest ion dose is not the center of the groove but offset toward the side of the sample platen. Due to the sample plate and rod, many ions from below cannot reach the upper side of the groove, thus giving rise to lower doses on the upper half. The ion dose along the groove becomes more nonuniform with time because the areas close to the edges receive progressively a larger number of glancing incident ions.

B. Experimental results

Figure 6 displays the nitrogen depth profiles of the five samples measured by AES. Samples 2 and 3 show the deepest projected range, R_p, at about 56 nm. Samples 5 and 1 have the smallest projected range at about 12 nm. Our experimental results indicate that the projected range is smaller toward the edge and agree with the simulation results described in the previous section. A closer look at the depth profiles also reveals that samples 4 and 5 (upper side) have smaller projected ranges than those on the lower side (samples 1 and 2). The results are also in good agreement with our simulation. The penetration depth of the implanted ions depends on the energy and incident angle of the ions. When the ion impact angle becomes more oblique, the implantation is naturally shallower.

The retained doses in the samples are plotted in Fig. 7. Sample 2 has the largest retained dose, about 2.2

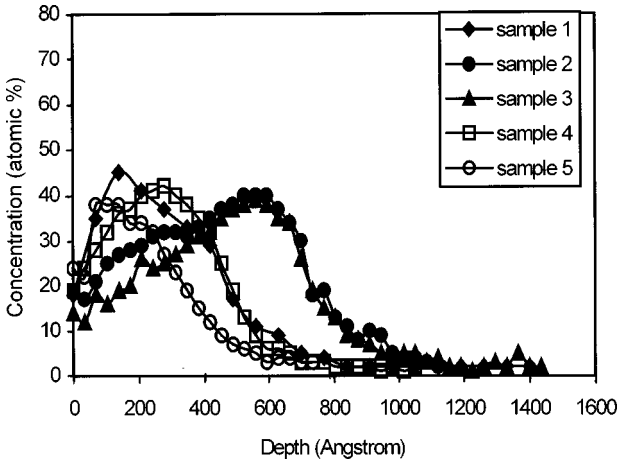

FIG. 6. Experimental nitrogen depth profiles acquired from the five stainless steel sheets shown in Figs. 1 and 2 by Auger electron spectroscopy depth profiling.

$\times 10^{17}$ ions/cm^2. The minimum retained dose, 1.2 $\times 10^{17}$ ions/cm^2, is calculated from sample 5. Similar to our simulation results, the retained dose near the groove edge is also much smaller than that near the center. In addition, the maximum retained dose is observed not on the bottom of the arc trench (sample 3), but in the area close to supporting plate (sample 2). The distribution of the retained dose is not symmetrical about the center of the groove. Samples 4, 5 (upper side) have smaller retained dose values compared to samples 1 and 2 (lower side). It can therefore be inferred that the upper edge is the most challenging location to maintain implantation uniformity. The maximum retained dose nonuniformity is calculated to be about 40% along the groove.

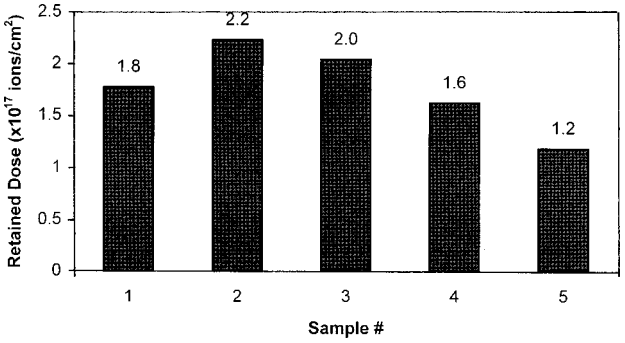

FIG. 7. Calculated retained doses of the five stainless steel pieces shown in Figs. 1 and 2.

Our simulation and experimental results agree very closely and illustrate the practical uniformity achievable on industrial bearings with inner grooves.

V. CONCLUSION

Our experimental and theoretical simulation results reveal ion dose and projected range variation along the working surface of a bearing inner race. In the groove, the maximum ion dose is not in the middle or bottom of the arc groove but slightly displaced toward the side of the sample platen if the bearing is laid horizontally on the sample stage. The edges show lower doses as well as shallower projected ranges. The more oblique incident angle near the edge of groove spurs enhanced sputtering (i.e., lower retained dose) and results in shallower projected ranges. Due to the horizontal placement of the bearing on the sample platen, the upper side of the groove receives a smaller ion dose compared to the lower side. The variation along the groove surface is about 40% based on our Auger results. An obvious means to minimize the difference between the upper and lower half of the bearing is to stack several bearings on top of each other to normalize the effects. However, this will increase the current demand on the power modulation as the total implantation area is increased. Better conformality can also be achieved by increasing the plasma density at the same nitrogen pressure (a high pressure will reduce the ion mean free path and increase collisions thereby reducing the net ion impact energy). This can be accomplished by using a more efficient ion source but care must be taken not to compromise the plasma uniformity excessively.

ACKNOWLEDGMENTS

The work was supported by Hong Kong Research Grants Council projects 9040332 and 9040344.

[1] J. R. Conrad, J. L. Radtke, R. A. Dodd, F. J. Worzala, and N. C. Tran, J. Appl. Phys. **62**, 4591 (1987).
[2] G. A. Collins, R. Hutchings, J. Tendys, and M. Samandi, Surf. Coat. Technol. **68/69**, 285 (1994).
[3] J. R. Conrad, R. A. Dodd, S. Han, M. Madapura, J. Scheuer, K. Sridharan, and F. J. Worzala, J. Vac. Sci. Technol. A **8**, 3146 (1990).
[4] S. Y. Wang, P. K. Chu, B. Y. Tang, X. C. Zeng, and X. F. Wang, Nucl. Instrum. Methods Phys. Res. B **127**, 100 (1997).
[5] M. Hirano and S. Miyake, Appl. Phys. Lett. **49**, 779 (1986).
[6] P. K. Chu, B. Y. Tang, Y. C. Cheng, and P. K. Ko, Rev. Sci. Instrum. **68**, 1866 (1997).
[7] M. Hong and G. A. Emmert, J. Appl. Phys. **78**, 8967 (1995).
[8] T. E. Sheridan and M. J. Alport, J. Vac. Sci. Technol. B **12**, 897 (1994).
[9] M. Windner, I. Alexeff, W. D. Jones, and K. E. Lonngren, Phys. Fluids **13**, 2532 (1970).
[10] T. E. Sheridan, J. Phys. D **29**, 2725 (1996).
[11] M. Hong and G. A. Emmert, J. Vac. Sci. Technol. B **12**, 889 (1994).
[12] T. E. Sheridan, Appl. Phys. Lett. **64**, 1783 (1994).